

JGR Biogeosciences

RESEARCH ARTICLE

10.1029/2019JG005022

Key Points:

- Correlation between photochemical reflectance index (PRI) and carbon fluxes were assessed for a subtropical mangrove wetland
- Diurnal and seasonal mangrove PRI variations were significantly correlated with meteorological and photosynthetic variables
- PRI performed better than normalized difference vegetation index (NDVI) in tracking mangrove photosynthetic phenology

Supporting Information:

- Supporting Information S1
- Data Set S1
- Data Set S2

Correspondence to:

X. Zhu,
xdzhu@xmu.edu.cn

Citation:

Zhu, X., Song, L., Weng, Q., & Huang, G. (2019). Linking in situ photochemical reflectance index measurements with mangrove carbon dynamics in a subtropical coastal wetland. *Journal of Geophysical Research: Biogeosciences*, 124. <https://doi.org/10.1029/2019JG005022>

Received 10 JAN 2019

Accepted 16 MAY 2019

Accepted article online 31 MAY 2019

Author Contributions:

Conceptualization: Xudong Zhu

Data curation: Guanmin Huang

Formal analysis: Xudong Zhu, Lulu Song, Qihao Weng

Funding acquisition: Xudong Zhu

Investigation: Xudong Zhu, Qihao Weng, Guanmin Huang

Methodology: Xudong Zhu, Lulu Song, Qihao Weng

Project administration: Xudong Zhu

Validation: Lulu Song, Guanmin Huang


Visualization: Xudong Zhu

Writing - original draft: Xudong Zhu

Writing - review & editing: Xudong Zhu, Lulu Song, Qihao Weng

©2019. American Geophysical Union.
All Rights Reserved.

Linking In Situ Photochemical Reflectance Index Measurements With Mangrove Carbon Dynamics in a Subtropical Coastal Wetland

Xudong Zhu¹ , Lulu Song², Qihao Weng³ , and Guanmin Huang⁴

¹Key Laboratory of the Coastal and Wetland Ecosystems (Ministry of Education), Coastal and Ocean Management Institute, College of the Environment and Ecology, Xiamen, China, ²Key Laboratory of Urban Environment and Health, Institute of Urban Environment, Chinese Academy of Sciences, Xiamen, China, ³Center for Urban and Environmental Change, Department of Earth and Environmental Systems, Indiana State University, Terre Haute, IN, USA, ⁴Administrative Bureau of Zhangjiang Estuary Mangrove National Nature Reserve, Yunxiao, China

Abstract Photochemical reflectance index (PRI) has been found to be closely related with vegetation photosynthetic phenology in many ecosystems including boreal evergreen, but its ability to track carbon dynamics in low-latitude evergreen mangrove ecosystems has rarely been assessed. To fill up this gap, this paper explored potential mangrove PRI-carbon links and their environmental controls across temporal scales (diurnal and seasonal), based on 1-year continuous high-resolution (half-hourly) time series measurements of spectral signals, eddy covariance carbon fluxes, and multiple environmental factors at a subtropical mangrove wetland of southeastern China. The diurnal variation of half-hourly mangrove PRI, a U-shaped changing pattern, was consistent with previous PRI studies on boreal evergreen, while the seasonal variation of daily mangrove PRI did not experience a hump-shaped changing pattern as in boreal evergreen. Diurnal and seasonal mangrove PRI variations were significantly correlated with meteorological (radiation and vapor pressure deficit) and carbon-related parameters (gross primary productivity, net ecosystem exchange, and light use efficiency), and the strength of diurnal PRI-carbon correlations varied with meteorological factors with stronger correlations at enhanced radiation and vapor pressure deficit. Our results further indicated that physiology-related PRI performed better than conventional structure-related normalized difference vegetation index in tracking mangrove photosynthetic parameters. To the best of our knowledge, this is the first study to explore the link between high-frequency PRI and carbon dynamics across temporal scales in natural mangrove ecosystems. The PRI-carbon linkage confirmed by this study will improve our understanding of temporal variations in photosynthetic carbon dynamics in mangrove ecosystems.

1. Introduction

Mangrove is one of the most important coastal blue carbon ecosystems with strong carbon sequestration potential (Nellemann & Corcoran, 2009) to mitigate climate change dominated by anthropogenic activities, such as industrial carbon emissions and land cover/use changes (Le Quéré et al., 2009). Mangrove is characteristic of high and effective carbon sink due to slower sediment decomposition and higher carbon accumulation under anoxic environment over the intertidal zone (Atwood et al., 2017; Howard et al., 2017), but the temporal variation and spatial heterogeneity of mangrove carbon fluxes are extremely high (Alongi, 2012, 2014). Surface-atmospheric carbon fluxes have been quantified using a number of measuring and modeling techniques, among which eddy covariance (EC; Baldocchi et al., 2001) has been increasingly used as a primary tool to provide near-direct assessment of in situ carbon fluxes for different ecosystems including mangrove wetlands (Barr et al., 2010; Cui et al., 2018). EC provides an excellent means of sampling surface-atmospheric carbon exchanges at fine temporal scale (usually half-hourly), but limited spatial coverage and high instrument/infrastructure costs make it challenged for more spatially extensive applications. Instead, satellite and aerial remote sensing, as complementary observation techniques to EC, provides an ideal opportunity to spatially upscale carbon flux measurements from sampling footprint extents (usually <1 km²) to regional and global scales.

Historically, vegetation remote sensing has been more focused on mapping and monitoring spatial and temporal patterns of vegetation types and their biophysical parameters (e.g., leaf area index, Tian et al., 2002; greenness-based phenology, Tucker et al., 1985), but recent development of vegetation remote sensing has moved beyond these structure-related parameters to more function-related ones (e.g., gross primary productivity [GPP], Frankenberg et al., 2011; light use efficiency [LUE], Zhang et al., 2017; water use efficiency, Wagle et al., 2016; and leaf nitrogen concentration, Zhang et al., 2013), providing a better understanding of underlying ecosystem physiological responses. Among these remote sensing applications, vegetation production estimation based on LUE models has become one of the most widely reported applications (Garbulsky et al., 2008; Gitelson & Gamon, 2015; Xiao et al., 2004; Yuan et al., 2007). Basically, LUE-based vegetation production models state that GPP is a product of incident photosynthetically active radiation (PAR), fraction of absorbed PAR (f_{APAR} ; proportional to green leaf area), and LUE (Monteith & Moss, 1977; Ruimy et al., 1994). PAR is typically obtained from meteorological data, and the latter two are often linked to remote sensing spectral indices. For deciduous or annual vegetation, the seasonality of photosynthetic activity, or photosynthetic phenology (Gamon et al., 2016), is coupled with the seasonality of green leaf area and f_{APAR} . Thus, vegetation indices (e.g., normalized difference vegetation index [NDVI], Myneni & Williams, 1994; and enhanced vegetation index, Huete et al., 2002), responsive to changes in green leaf area, can be used to capture the seasonal dynamics of vegetation production (Running et al., 2004). But, for evergreen vegetation (e.g., mangrove), relatively stable greenness over the year is decoupled with photosynthetic phenology (Barr et al., 2013), which is more governed by LUE varying in time and space with environmental stresses (Garbulsky et al., 2010; Garbulsky et al., 2011). Therefore, it is appealing to assess LUE and photosynthetic phenology directly from remote sensing to track the seasonality of vegetation production especially for evergreen vegetation.

To better characterize vegetation photosynthetic phenology, many satellite and proximal remote sensing approaches have been recently developed from a variety of sensors. A recent emerging approach is based on the link between GPP and Sun-induced chlorophyll fluorescence (SIF), which is derived from atmospheric oxygen absorption bands where small fluorescence signals can be detected from large background solar radiation (Porcar-Castell et al., 2014). Although strong SIF-GPP linkage has been demonstrated from spaceborne remote sensing at coarse temporal and spatial scales (Frankenberg et al., 2011; Joiner et al., 2014; Walther et al., 2016), this SIF-GPP hypothesis has not been well confirmed for proximal SIF applications across vegetation types, mainly due to the difficulty in detecting and interpreting weak SIF signals (Gamon, 2015; Porcar-Castell et al., 2014; Shrestha et al., 2012; Yang et al., 2018). Another promising approach to remotely assess photosynthetic phenology is based on photochemical reflectance index (PRI), which is sensitive to diurnal and seasonal changes in vegetation pigment contents (Gamon et al., 1992). Different from SIF that is essentially of continuous signal over the spectrum, PRI is a simple two-band index to describe relative magnitude of the reflectance of two narrow bands in sensitive (usually centered on 531 nm; ρ_{531}) and referenced (usually centered on 570 nm; ρ_{570}) spectral region. The close relationship between PRI and photosynthetic phenology has been widely documented with different vegetation types from both proximal and satellite applications (Garbulsky et al., 2011).

The temporal variation in PRI time series is thought to reflect the combined changes in pigment composition (xanthophyll cycle) and its pool size (chlorophyll and carotenoid contents), which dominate alternatively at various temporal scales (Gamon, 2015). At diurnal scale with constant pigment pool size, PRI tends to show a U-shaped diurnal pattern governed by nonradiative energy dissipation via xanthophyll cycle (Demmig et al., 1987; Gamon et al., 1992), in which excessive absorbed PAR causes the de-epoxidation of violaxanthin to zeaxanthin, leading to lower ρ_{531} but unaffected ρ_{570} (thus lower PRI). In contrast, at seasonal scale, PRI tends to show a hump-shaped seasonal pattern, since PRI also serves a relative chlorophyll-carotenoid index comparing the reflectance in the blue (chlorophyll and carotenoid absorption) and red (chlorophyll absorption only) spectral region. Long-term seasonal PRI variations in many ecosystems might be more influenced by the changes in pigment pool size (e.g., higher chlorophyll-carotenoid ratio in growing seasons) than the diurnal adjustment by xanthophyll cycle (Filella et al., 2009; Gamon et al., 2016). Although it is still challenging to differentiate these short-term and long-term effects on the PRI signal, the responses of PRI to the changes in both facultative xanthophyll cycle and constitutive pigment pool size ensure that PRI may serve an effective spectral index to track photosynthetic phenology especially for evergreen vegetation where

conventional structure-dependent vegetation indices (e.g., NDVI) are temporally decoupled with photosynthetic phenology.

Mangrove is typically evergreen vegetation in tropical and subtropical coastal wetlands that experiences a number of environmental stresses, including periodical tidal inundation (Cruse et al., 2013), high soil salinity (Song et al., 2011), low temperature (Chen et al., 2017), excess light absorption (Ball, 1996), and wastewater pollution (Jiang et al., 2018). It is difficult to accurately assess mangrove carbon fluxes that vary a lot both in time and space, partially because all of the environmental stresses are temporally varying and/or spatially heterogeneous (Alongi, 2014). In addition, it is impractical to manually monitor mangrove forests on a regular basis since the accessibility to and field survey of mangrove forests are notoriously difficult due to flooded and soft sediment surfaces usually full of stems and prop roots. Given these challenges, remote sensing provides an operational alternative to monitor mangrove carbon dynamics (Giri, 2016; Simard et al., 2019). Although PRI has been confirmed to have the ability of capturing photosynthetic capacity at leaf, canopy, and ecosystem scales for many vegetation types (Garbulsky et al., 2011), the linkage between PRI and carbon dynamics in natural mangrove ecosystems has rarely been reported. Nichol et al. (2006) explored the diurnal relationships between PRI and several photosynthetic measurements and confirmed PRI was an effective indicator of mangrove photosynthetic activity, but their continuous spectral measurements were too short to reveal any seasonal pattern. Also, the study was conducted on experimental mangrove canopy in the laboratory without suffering periodical tidal activities, and thus their findings might not accurately reflect the pattern in the field. Song et al. (2011) identified a strong link between PRI and salinity gradient in natural mangrove ecosystems, but their study lacked long-term continuous PRI measurements and did not directly examine the link between PRI and photosynthetic activities. S. Yang et al. (2018) also found a strong correlation between PRI and LUE in a natural mangrove forest based on 2-month in situ measurements, but they were unable to assess the correlation at seasonal scale. To date, the ability of PRI to track photosynthetic phenology across temporal scales in natural mangrove ecosystems has yet to be fully assessed.

Although the linkage between PRI and carbon dynamics of evergreen vegetation has already been confirmed by many studies (Garbulsky et al., 2011), most of them focus on evergreen vegetation experiencing boreal climate (e.g., evergreen conifers). It is unclear whether the diurnal and seasonal PRI-carbon relationships in boreal evergreen are applicable to subtropical/tropical evergreen like mangrove. First, in comparison with boreal climate, stronger atmospheric interference including cloudiness and aerosols usually leads to poorer PRI-carbon relationships in subtropical/tropical areas (Garbulsky et al., 2011). Second, with low stomatal conductance and intercellular CO₂ levels (Alongi, 2009), mangroves tend to have saturated photosynthetic rates at comparatively low light levels (Ball, 1996), which might obscure mangrove PRI-carbon relationships at diurnal scale. Third, with habitats at low latitudes and proximal to the sea, mangroves are experiencing much smaller annual temperature ranges than boreal evergreen, and thus the effects of constitutive pigment pool size on PRI variations might not be obvious at seasonal scale. In this study, based on continuous high-frequency measurements of PRI and EC at a mangrove flux tower at a subtropical mangrove wetland of southeastern China, we explored the relationship between in situ PRI and mangrove photosynthetic phenology, aiming to answer the following science questions: (1) How do in situ PRI measurements respond to environmental conditions at both diurnal and seasonal scales? (2) Can in situ PRI measurements capture diurnal and seasonal variations in mangrove carbon dynamics? And (3) how do environmental controls affect PRI-carbon relationships?

2. Materials and Methods

2.1. Study Site

The in situ measurements of this study were conducted at a mangrove flux station (Figure 1) located in a subtropical estuarine wetland of southeastern China, administrated by Zhangjiang Estuary Mangrove National Nature Reserve, Fujian, China. Based on historical climate data over 1960–1999, the mangrove wetland has a monsoon climate with annual mean rainfall of 1,714.5 mm mostly occurring from April to September and has an annual mean air temperature of 21.2 °C and annual mean relative humidity of 79% (Lin, 2001). The mangrove forests (Figure 1) have close canopy structure (Li et al., 2014) with average height of 3.1 m, average leaf area index of 1.7 m²/m², and species composition (Zhu et al., 2019) of *Kandelia obovate*

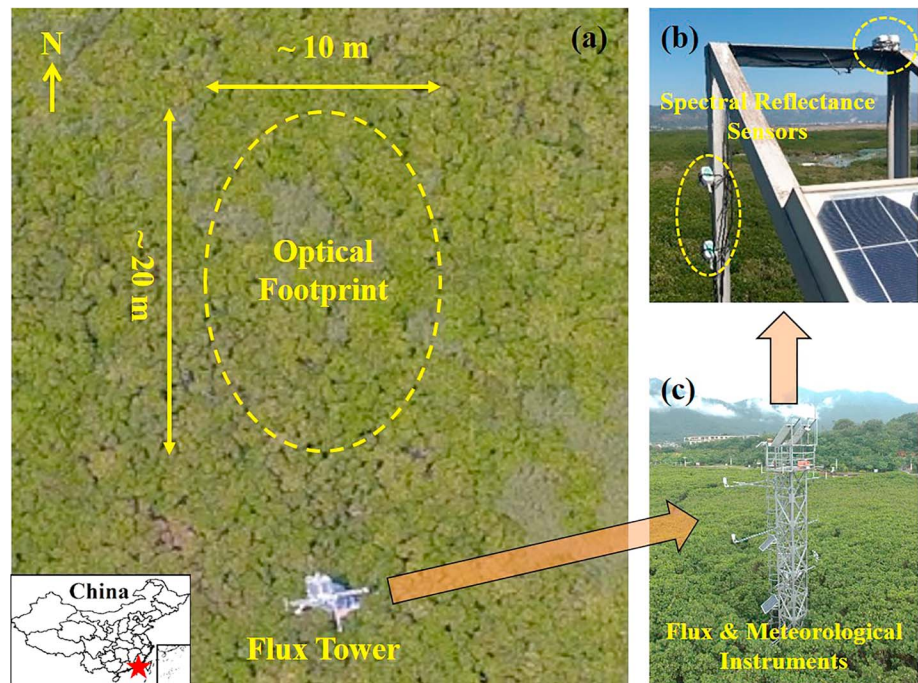


Figure 1. Experimental setup of in situ measurements in a subtropical estuarine mangrove wetland of southeastern China: (a) aerial view of mangrove forests near flux tower overlaid with approximate footprint (dashed ellipsoid) of spectral reflectance sensors deployed on the top of flux tower (b), and (c) flux and meteorological instruments deployed on the flux tower.

(67.5% in areal proportion), *Avicennia marina* (12.1%), and *Aegiceras corniculatum* (20.4%). The mangrove wetland experiences an irregular semidiurnal tide with an annual mean tide range of 2.32 m and is usually inundated twice per day. High tides can reach up to ~1 m above sediment surface at the flux tower, and the sediment surface is also exposed for days during the annual minima. Controlled by the mixing of downstream tidal water, upstream river water and rainfall, the salinity of surface water within the mangrove wetland ranges from 0 to 15 ppt. All necessary permits on in situ research activities in this study were acquired from the Zhangjiang Estuary Mangrove National Nature Reserve Administration, and more details on biotic and abiotic resources of the reserve can be found in Lin (2001).

2.2. Spectral Measurements and Calculations

Canopy spectral measurements for calculating canopy PRI and NDVI were collected using Spectral Reflectance Sensors (SRS; Decagon Devices, Pullman, WA, USA) mounted in fixed locations on the top of the flux tower (Figure 1b). For the calculation of canopy PRI (equation (1); Gamon et al., 1992), a pair of upward and downward facing SRS sensors were used to respectively measure incoming (I_L , $W \cdot m^{-2} \cdot nm^{-1}$) and reflected (I_F , $W \cdot m^{-2} \cdot sr^{-1} \cdot nm^{-1}$) radiation flux density at two narrow (full width half maximum = 10 nm) bands centered at 531 and 570 nm. Similarly, for canopy NDVI (equation (2)), another pair of upward and downward facing SRS sensors were used centered at 650 and 810 nm (full width half maximum = 10 nm). The downward facing SRS sensors had a field of view of 36° measuring canopy reflected radiation, and the upward facing SRS sensors built with Teflon cosine-corrected diffusers had a hemispherical field of view measuring incident radiation. Both sets of SRS sensors were affixed at ~9 m above the top of the mangrove with mean canopy height of ~6 m, and downward facing sensors were mounted facing north with 45° view zenith angle. Spectral measurements (I_L and I_F) were recorded on a CR3000 data logger (Campbell Scientific, Inc., Logan, UT, USA) and calculated as half-hourly averages. Canopy reflectance in the specific wavelength (ρ) was calculated as $\pi \times I_F/I_L$.

$$PRI = (\rho_{531} - \rho_{570}) / (\rho_{531} + \rho_{570}) \quad (1)$$

$$NDVI = (\rho_{810} - \rho_{650}) / (\rho_{810} + \rho_{650}) \quad (2)$$

2.3. Meteorological and Tidal Measurements

Meteorological measurements involved in this study, from multiple instruments on the flux tower (Figure 1c), include incoming shortwave radiation (SW_{in}), outgoing shortwave radiation (SW_{out}), PAR, air temperature, relative humidity, rain, wind speed, and soil temperature. SW_{in} and SW_{out} were measured using CNR4 Net Radiometer (Kipp & Zonen, Delft, Netherlands) at a height of ~12 m above the ground, and PAR were measured using PQS1 PAR Quantum sensors (Kipp & Zonen, Delft, Netherlands) at the same height. SW_{in} was used to calculate clearness index, which is the ratio of daily SW_{in} and daily extraterrestrial radiation (Zhu et al., 2010). Air temperature and relative humidity were measured at a height of ~9 m using a HMP155A sensor (Vaisala, Helsinki, Finland). Air temperature and relative humidity were combined to calculate vapor pressure deficit (VPD; Murray, 1966). Rain and wind speed (at ~9 m) were recorded using TE525MM Rain Gage (Campbell Scientific, Inc., Logan, UT, USA) and 010C Wind Speed Sensor (Met One Instruments, Inc., OR, USA), respectively. Soil temperature at the depth of 0.20 m was measured using soil thermocouple probe (model 109, Campbell Scientific, Inc., Logan, UT, USA). All meteorological measurements were recorded on a CR1000 data logger (Campbell Scientific, Inc., Logan, UT, USA). Tidal surface water level and salinity were, respectively, estimated from measurements using HOBO U20L-04 Water Level Logger and U24-002-C Conductivity Logger (Onset, Bourne, MA, USA) deployed just above ground surface near the flux tower. All meteorological and tidal measurements were consistently converted to half-hourly data for further analysis.

2.4. Carbon Flux Measurements and Data Processing

Carbon fluxes between the atmosphere and mangrove canopy were measured by the EC method with a three-axis sonic anemometer (CSAT-3, Campbell Scientific, Inc., Logan, UT, USA) and an open path infrared gas analyzer (LI-7500, Li-COR Inc., Lincoln, NE, USA), which were mounted at a height of ~1 m above the canopy (Figure 1c). Raw EC data at 10 Hz were recorded on a CR3000 data logger (Campbell Scientific, Inc., Logan, UT, USA) and stored on a built-in flash card for further data processing.

The procedure of EC data processing and calculations contained several steps pertinent to flux calculation and correction, data quality control, and flux partition. First, raw EC data at 10 Hz were processed and corrected to derive half-hourly net ecosystem exchange (NEE; 74.5% data availability) in EddyPro6.1 (Li-COR Inc., Lincoln, NE, USA), a data processing software for eddy flux calculation and correction, including axis rotation, ultrasonic correction, and frequency response correction. Second, multiple flux quality control procedures (including steady state test, turbulent conditions test, statistical tests, absolute limits test, and rain test) were applied in EddyPro6.1 to remove NEE data with poor quality (44.2% data availability). Third, a threshold of friction velocity of 0.1 m/s, calculated as in Reichstein et al. (2005), was used to filter out nighttime (incoming shortwave radiation $< 20 \text{ W/m}^2$) flux measurements under insufficient turbulence (42.8% data availability). Fourth, nighttime NEE (or nighttime ecosystem respiration, $R_{eco}(t)$) and soil temperature ($T(t)$) were used to estimate temperature sensitivity (E_0) and time-dependent reference respiration ($R_{ref}(t)$) in the exponential regression model (equation (3); Lloyd & Taylor, 1994), using the short-term temperature sensitivity algorithm with the reference respiration (T_{ref}) and the regression parameter (T_0) set to 10 °C and - 46.02 °C, respectively (see Reichstein et al., 2005, for details on the algorithm). Fifth, the fitted temperature-respiration exponential regression model was extrapolated to derive daytime $R_{eco}(t)$ from daytime $T(t)$, and then GPP was estimated from daytime NEE (equation (4)). Sixth, the LUE (equation (5)) was calculated as the ratio of GPP and absorbed PAR (APAR; the product of PAR and f_{APAR} ; equation (6)), where f_{APAR} was derived from SW_{in} and SW_{out} (equation (7); Nichol et al., 2019). The sign convention used in meteorology (i.e., the downward flux is negative and the upward one is positive) was used for indicating carbon fluxes.

$$R_{eco}(t) = R_{ref}(t)e^{E_0(1/(T_{ref}-T_0)-1/(T(t)-T_0))} \quad (3)$$

$$GPP(t) = NEE(t) - R_{eco}(t) \quad (4)$$

$$LUE(t) = |GPP(t)| / APAR(t) \quad (5)$$

$$APAR(t) = PAR(t) \times f_{APAR}(t) \quad (6)$$

$$f_{APAR}(t) = 1 - SW_{out}(t) / SW_{in}(t) \quad (7)$$

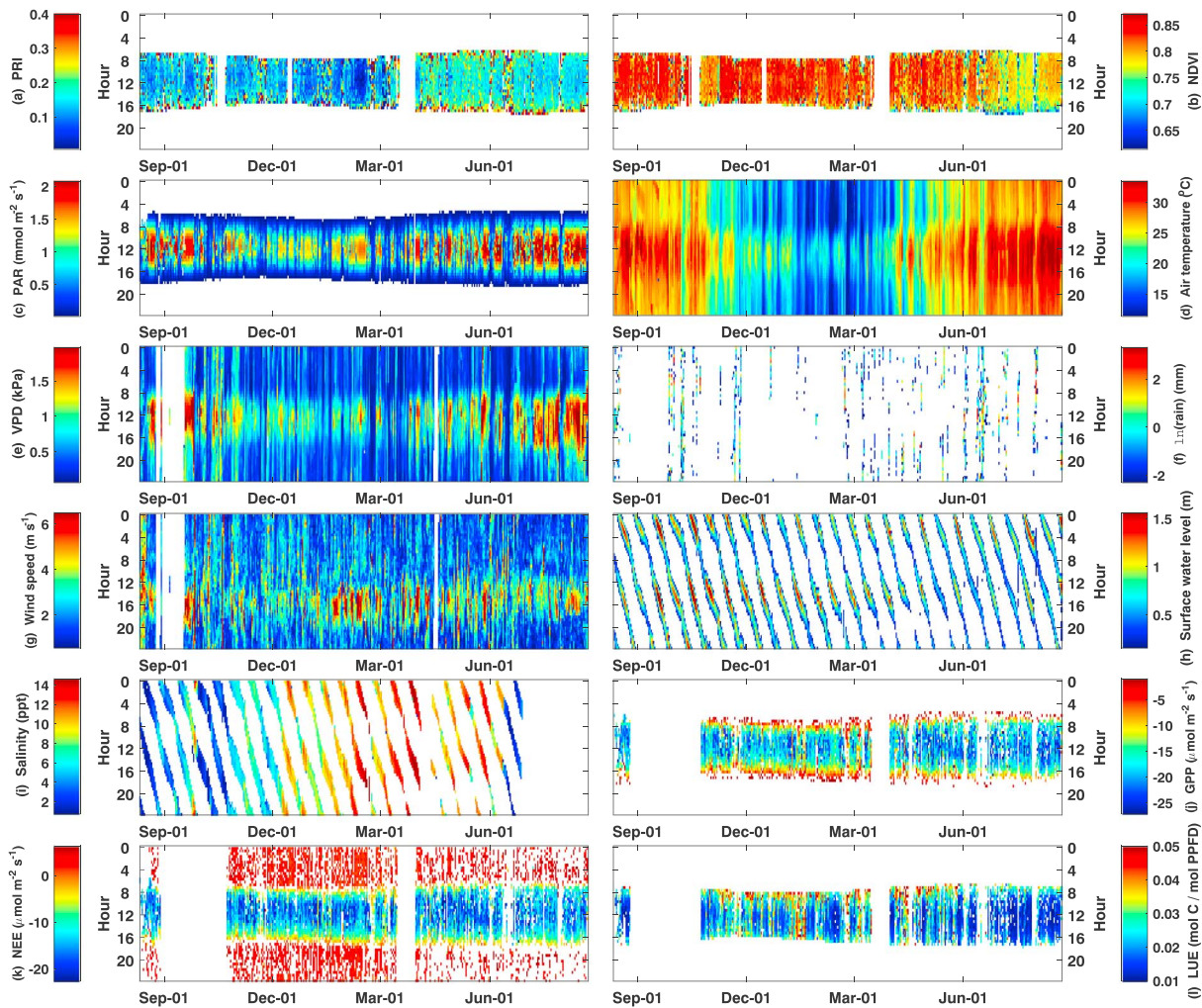


Figure 2. Diurnal and seasonal variations in half-hourly measurements of spectral (a, b: photochemical reflectance index and normalized difference vegetation index), meteorological (c–g: photosynthetically active radiation, air temperature, vapor pressure deficit, rain, and wind speed), tidal (h, i: surface water level and salinity), and carbon (j–l: gross primary production, net ecosystem exchange, and light use efficiency) variables from August 2016 to August 2017. Note the natural logarithm of rain was shown for better visibility. PRI = photochemical reflectance index; NDVI = normalized difference vegetation index; PAR = photosynthetically active radiation; VPD = vapor pressure deficit; GPP = gross primary production; NEE = net ecosystem exchange; LUE = light use efficiency.

2.5. Statistical Analysis

To exclude potential abnormal spectral signals at dawn or dusk (Soudani et al., 2014), only half-hourly spectral data of PRI and NDVI with instantaneous solar elevation $>15^\circ$ (Zhang et al., 2017) were used for further analysis at the diurnal scale. This criterion was also applied to the estimation of half-hourly LUE to avoid data with bad quality at low light conditions. For the analysis at seasonal scale, only half-hourly data (spectral, meteorological, tidal, and carbon flux measurements) acquired from 10:00 to 15:30 were used to calculate daily values to avoid abnormal values around early morning and late afternoon (Zhang et al., 2017). In addition, measurements on rainy days were excluded in data analysis due to inaccuracy of both spectral and flux measurements under rainy conditions. All data analyses were performed using MATLAB software (The MathWorks, Inc., MA, USA).

3. Results

3.1. Temporal Variations of In Situ PRI Measurements

The half-hourly PRI showed significant temporal variations, at both diurnal and seasonal scales, during the 1-year period from August 2016 to August 2017 (Figure 2a). The magnitude of half-hourly PRI typically

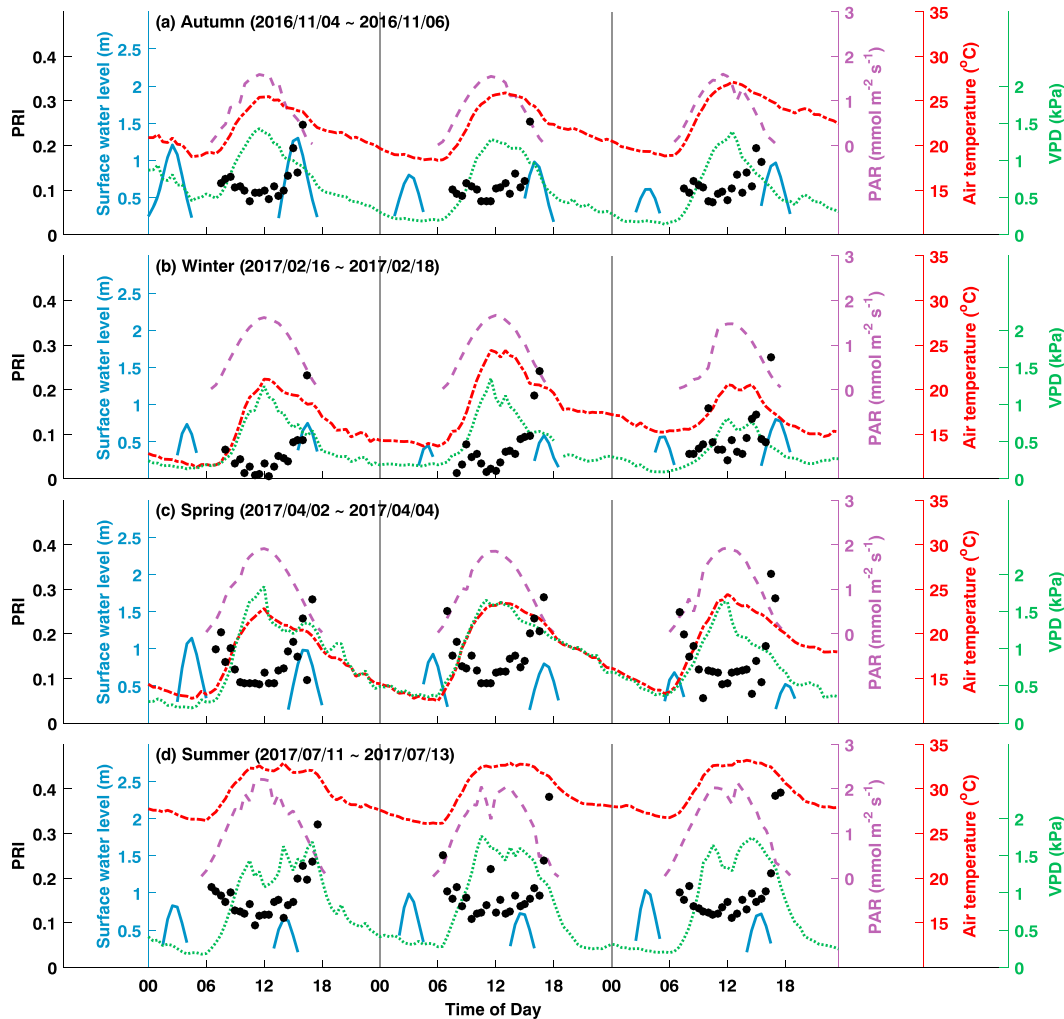


Figure 3. Diurnal variations in half-hourly PRI and environmental variables (surface water table, photosynthetically active radiation, air temperature, and vapor pressure deficit) over three consecutive days in each season. (a) Autumn, (b) winter, (c) spring, and (d) summer. PRI = photochemical reflectance index; PAR = photosynthetically active radiation; VPD = vapor pressure deficit.

varied from 0.01 to 0.40 with the average of 0.16. At diurnal scale, the half-hourly PRI tended to be lower during the hours around the noon; and at seasonal scale, the half-hourly PRI had higher values during spring (0.19 ± 0.08 ; mean \pm standard deviation) and summer (0.18 ± 0.08) months, but lower values during the winter (0.12 ± 0.08). To better illustrate typical diurnal patterns of in situ PRI measurements, three consecutive days were selected for each season to demonstrate typical diurnal responses of PRI (Figure 3). A visual examination of the PRI responses within four seasons indicated that PRI experienced a U-shaped diurnal pattern with low values around noon and high values in early morning and late afternoon. This U-shaped diurnal pattern persisted across the consecutive days and across seasons. The PRI values in the three consecutive days during the winter (< 0.05 around the noon) were obviously lower than those days during other seasons (> 0.1 around the noon). The daily PRI (average of half-hourly PRI), ranging from 0.05 to 0.48, also had a strong variation over the course of the year with statistically ($p < 0.01$) higher and lower mean daily values in spring (0.22) and winter (0.17), respectively (Figure 4a).

3.2. Response of In Situ PRI Measurements to Environmental Factors

Concurrent half-hourly time series of meteorological and tidal measurements (Figures 2c–2i) were used to examine how PRI signals responded to changing environmental conditions. The measurements of

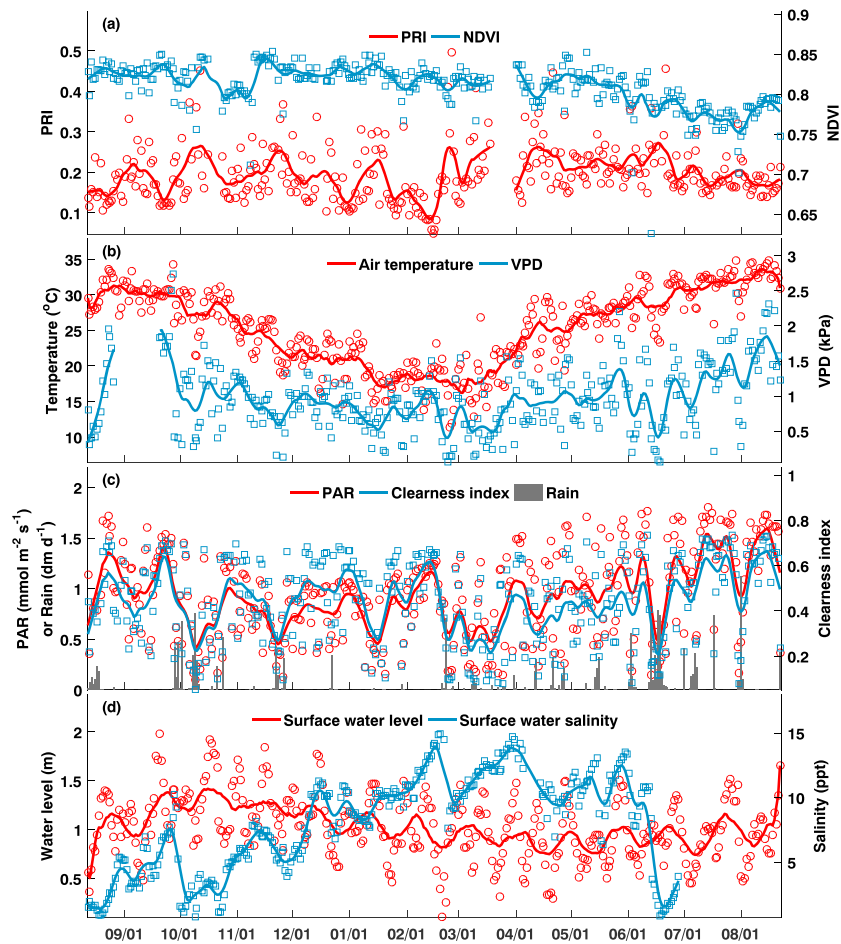


Figure 4. Seasonal variations in daily spectral (a: photochemical reflectance index and normalized difference vegetation index) and environmental variables (b: air temperature and vapor pressure deficit; c: photosynthetically active radiation, clearness index, and rain; d: maximum surface water level and mean surface water salinity) from August 2016 to August 2017. Lines indicate 15-day moving average of daily values. PRI = photochemical reflectance index; NDVI = normalized difference vegetation index; VPD = vapor pressure deficit; PAR = photosynthetically active radiation.

meteorological variables (PAR, air temperature, and VPD) had significant temporal variations. Half-hourly signals showed hump-shaped patterns at diurnal scale (Figure 3), while daily signals showed seasonal dynamics with higher (lower) values in summer (winter; Figures 4b and 4c). The temporal dynamics of half-hourly tidal surface water level reflected the Earth-Moon rhythm at diurnal scale (Figure 2h), and daily maximum surface water level was relatively higher in autumn and winter at seasonal scale (Figure 4d). Daily variation in surface water salinity was governed by daily precipitation, with higher values in spring months (Figures 4c and 4d). At diurnal scale, opposite changing patterns between PRI (U-shaped) and meteorological (hump-shaped) variables can be visually identified from half-hourly time series (Figure 3). Pearson correlation analysis indicated that half-hourly PRI was better correlated with PAR compared to air temperature and VPD (Figures 5a–5c). Pearson correlation coefficients (r) between half-hourly PRI and PAR calculated for each individual day were statistically significant ($p < 0.05$; same hereinafter) among 53.1% of valid days (excluding days with rain or missing data) over the study period, and this proportion reduced to 15.7% and 21.5% for air temperature and VPD, respectively (Table 1). Among the four seasons, spring and summer had larger proportion of valid days with inverse correlation between PRI and meteorological factors. At seasonal scale, the variation in daily PRI was found to be better explained by clearness index ($y = 0.40 - 0.44x/(x+0.50)$, $R^2 = 0.58$), PAR ($y = 0.48 - 0.40x/(x+0.36)$, $R^2 = 0.50$), and VPD ($y = 0.45 - 0.33x/(x+0.27)$, $R^2 = 0.29$) than air temperature and tidal factors (Figure 6).

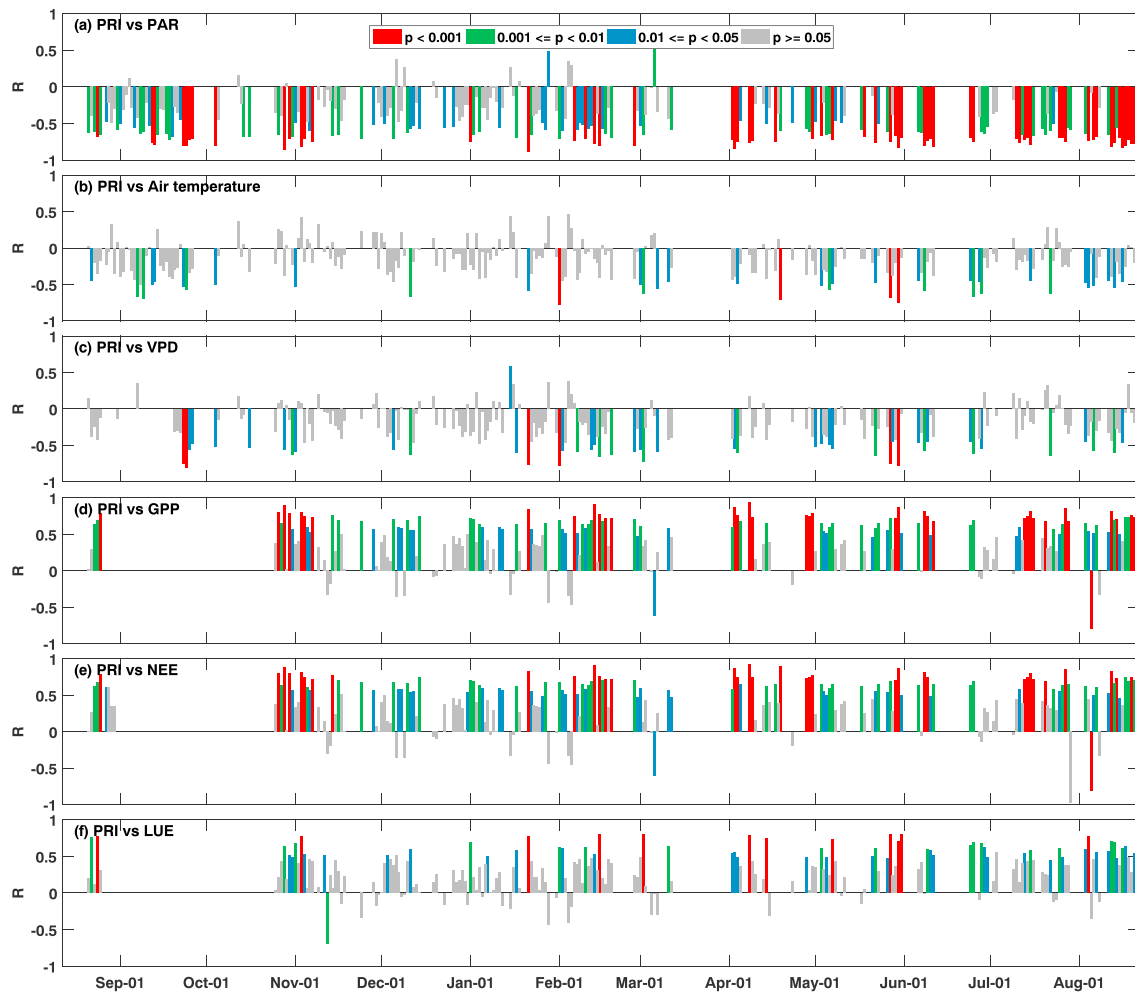


Figure 5. Person correlation coefficients between half-hourly PRI and meteorological and carbon variables for each individual nonrainy day. Bars with different colors denote different significance levels, and missing values result from insufficient measurements or rainy conditions. (a) PRI versus PAR, (b) PRI versus air temperature, (c) PRI versus VPD, (d) PRI versus GPP, (e) PRI versus NEE, and (f) PRI versus LUE. PRI = photochemical reflectance index; PAR = photosynthetically active radiation; VPD = vapor pressure deficit; GPP = gross primary production; NEE = net ecosystem exchange; LUE = light use efficiency.

Table 1

Percentage of Valid Days (Excluding Days With Rain or Missing Data) When Half-Hourly PRI and Meteorological/Carbon-Related Factors Were Significantly Correlated ($p < 0.05$)

Variables	Study period (2016/8/12 to 2017/8/22)	Autumn (2016/9/1 to 2016/11/30)	Winter (2016/12/1 to 2017/2/28)	Spring (2017/3/1 to 2017/5/31)	Summer (2017/6/1 to 2017/8/22)
PAR	53.1	44.6	44.2	62.8	60.2
Temperature	15.7	9.6	7.0	21.8	23.3
VPD	21.5	16.9	19.8	30.7	19.2
GPP	48.0	40.0	41.9	55.7	51.2
NEE	48.1	40.0	45.3	56.2	47.3
LUE	28.6	22.9	15.1	35.7	38.8

Note. Data are summarized for the whole study period and four seasons, and the largest percentage among seasons are highlighted in bold. PAR = photosynthetically active radiation; VPD = vapor pressure deficit; GPP = gross primary productivity; NEE = net ecosystem exchange; LUE = light use efficiency. Dates are formatted as year/month/day.

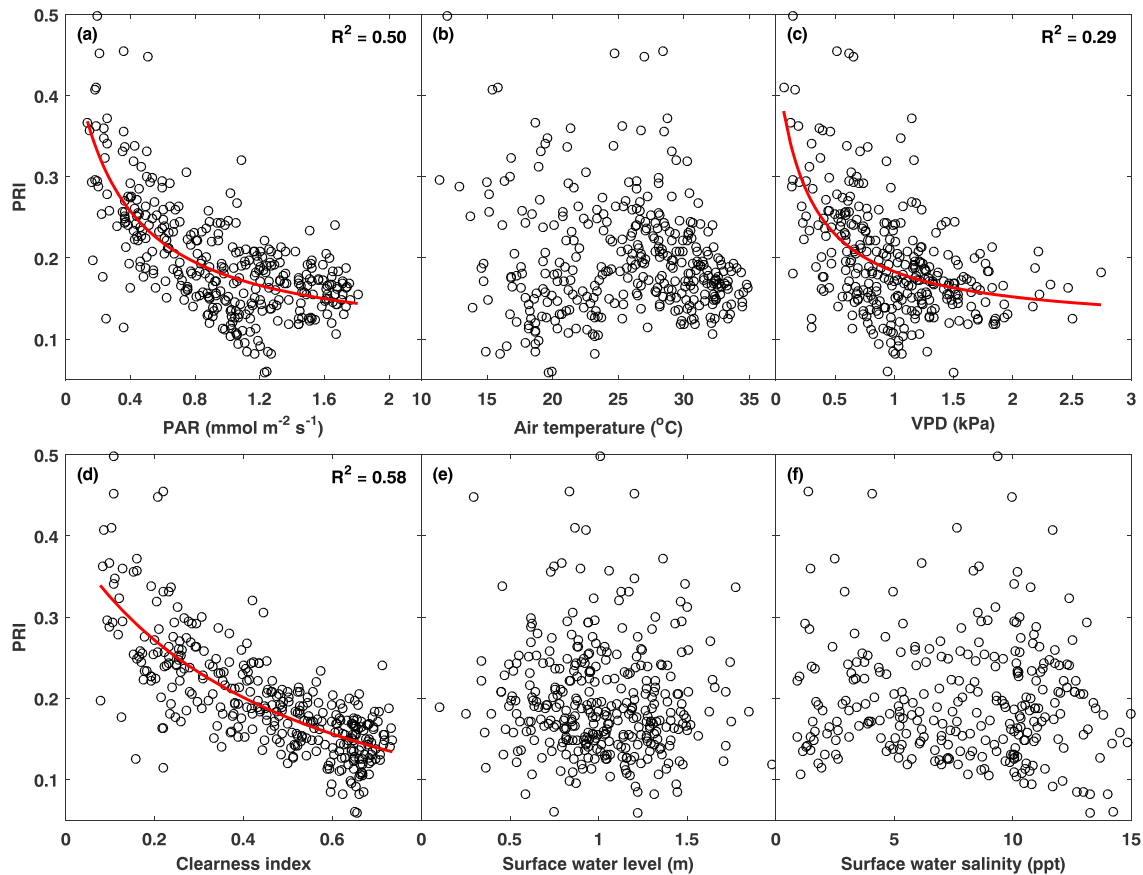


Figure 6. Scatter plots between daily PRI and environmental variables, including (a) daily PAR, (b) air temperature, (c) VPD, (d) clearness index, (e) surface water level, and (f) salinity. PRI = photochemical reflectance index; PAR = photosynthetically active radiation; VPD = vapor pressure deficit.

3.3. Correlations Between In Situ PRI Measurements and Mangrove Carbon Dynamics

Consistent with the environmental factors, half-hourly time series of GPP, NEE, and LUE (Figures 2j–2l) showed obvious temporal variations. All of these three variables showed U-shaped diurnal patterns (Figure 7). It is noted that negative values were used for daytime downward fluxes of GPP and NEE. Daily GPP and NEE shared similar seasonal variations with stronger carbon fluxes in spring and summer and weaker fluxes in autumn and winter, while daily LUE tended to be higher in winter and spring (Figure 8). PRI was found to covary well with the temporal dynamics of GPP, NEE, and LUE at both diurnal (Figure 7) and seasonal scales (Figure 8). Pearson correlation analysis based on half-hourly time series indicated that, at diurnal scale, the proportion of valid days when significantly positive correlation occurred is 48.0%, 48.1%, and 28.6% for GPP, NEE, and LUE, respectively (Figures 5d–5f and Table 1). Among four seasons, spring and summer had larger proportion of valid days with inverse PRI-carbon correlation (Table 1). At seasonal scale, daily PRI was also found to be positively related with GPP ($y = -19.3 + 29.4x$, $R^2 = 0.32$), NEE ($y = -23.5 + 31.6x$, $R^2 = 0.30$), and LUE ($y = 0.0072 + 0.069x$, $R^2 = 0.35$; Figure 9). Further analysis of environmental influences on PRI-carbon correlations indicated that the correlation coefficients between half-hourly PRI and carbon variables tended to be higher under enhanced PAR, VPD, and clearness index (Figure 10).

4. Discussion

The U-shaped diurnal pattern of half-hourly PRI identified from our high-frequency in situ spectral measurements in mangrove (Figures 3 and 5) conform to general understanding that short-term PRI-radiation relationship is physiologically controlled by plant photoprotective mechanism via xanthophyll pigment interconversion. This significant inverse PRI-PAR relationship at diurnal scale is consistent with previous

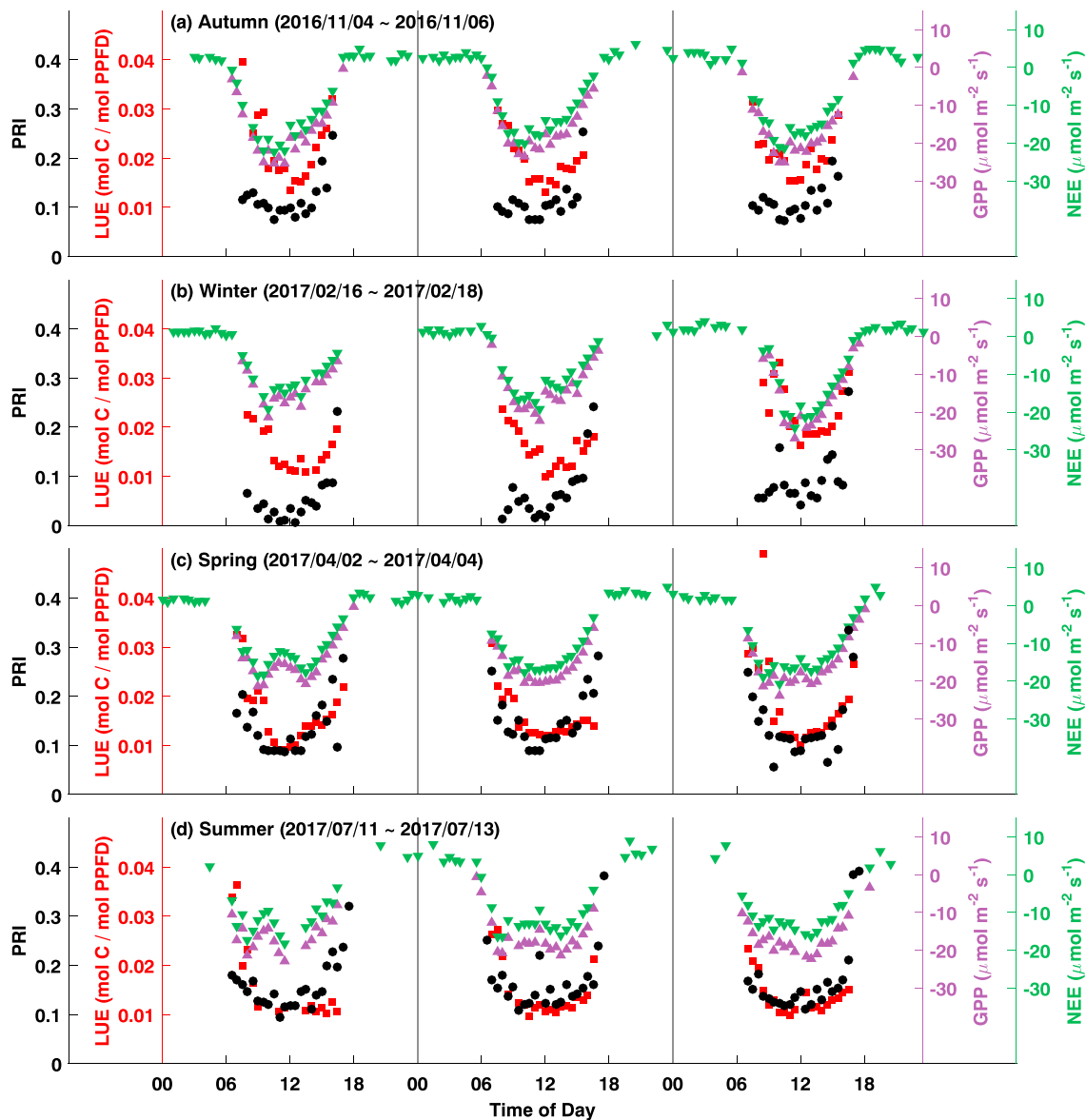


Figure 7. Diurnal variations in half-hourly PRI and carbon-related variables (light use efficiency, gross primary production, and net ecosystem exchange) over three consecutive days in each season. (a) Autumn, (b) winter, (c) spring, and (d) summer. PRI = photochemical reflectance index; LUE = light use efficiency; GPP = gross primary production; NEE = net ecosystem exchange.

empirical PRI studies in mangrove (Nichol et al., 2006) and many other vegetation types (Garbulsky et al., 2011). In addition to PAR, PRI variation was also found inversely related to the diurnal changes in VPD and air temperature (Figures 3 and 5), which is similar to the findings by Magney et al. (2016) that showed the diurnal magnitude of PRI increased with VPD and air temperature. Although it is hard to isolate individual effects from these meteorological factors with simultaneous diurnal changes, our correlation analysis suggests that PRI variation was more likely radiation-dominated with additional effects from atmospheric vapor and temperature conditions. This observation appears reasonable given that the presence of any environmental stresses including meteorological ones explored here can amplify radiation-induced down-regulation of PRI at short-term time scale (Hartel et al., 1996; Magney et al., 2016; Peguero-Pina et al., 2013). The stronger inverse correlation between PRI and PAR in spring and summer implies that the diurnal xanthophyll cycle might be more active in warmer seasons, which is consistent with several previous findings in boreal evergreen forests (Demmig-Adams et al., 2012; Verhoeven, 2014; Wong & Gamon, 2015). However, our results do not show much difference in PRI-PAR

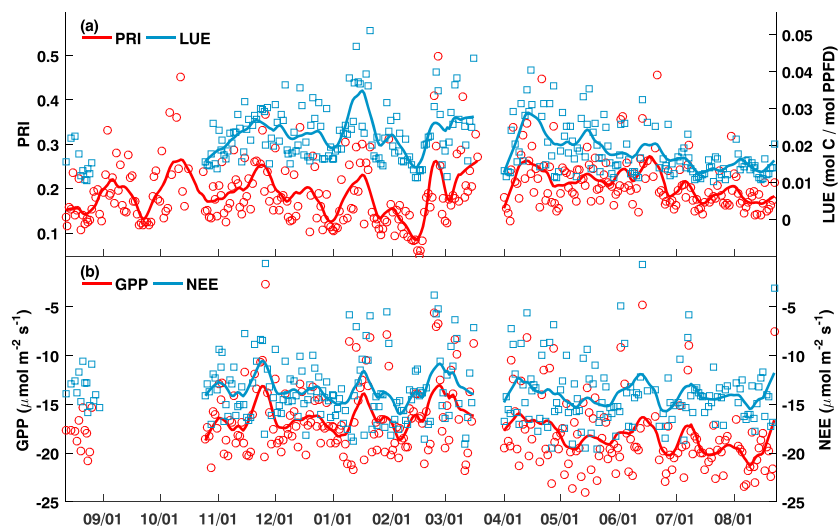


Figure 8. Seasonal variations in daily spectral and carbon-related variables (a: photochemical reflectance index and light use efficiency; b: gross primary production and net ecosystem exchange) from August 2016 to August 2017. Lines indicate 15-day moving average of daily values. PRI = photochemical reflectance index; LUE = light use efficiency; GPP = gross primary production; NEE = net ecosystem exchange.

correlations among seasons (in fact, >44% of valid days had significantly inverse PRI-PAR correlations for all seasons), due likely to the fact that subtropical mangrove experienced much smaller seasonal difference in temperature (~10 °C in our case) compared to evergreen forests in boreal climate (usually >20 °C).

The seasonality of daily PRI in mangrove ecosystems reveals that the varying range of daily PRI was small with spring (winter) having relatively higher (lower) values. It is likely that the difference in daily PRI among seasons was partially caused by the seasonal changes in pigment pool size as frequently stated by previous studies (Gamon et al., 2016), but this long-term pigment regulatory mechanism may play a minor role in determining the seasonality of PRI in subtropical mangrove ecosystems. The weak seasonal PRI difference in mangrove forests is not in agreement with the hump-shaped seasonal patterns from previous studies in boreal evergreens (Soudani et al., 2014; Wong & Gamon, 2015), but it is comparable to other subtropical forest types (Zhang et al., 2015; Zhang et al., 2017). These contrasting findings are reasonable given that there was much smaller seasonal temperature difference in subtropical evergreens compared to boreal evergreens. In fact, the varying ranges of daily PRI over weeks in our mangrove ecosystem were several times larger than the difference in seasonally mean daily PRI (Figure 4a), and daily PRI variations were tightly linked to daily PAR variations with PRI peaks (troughs) corresponding to PAR troughs (peaks; Figures 4a, 4c, and 6a). Daily PRI was also strongly correlated to clearness index, which is consistent with the findings by Zhang et al. (2017) focusing on evergreen forests in subtropical climate (Figure 6d). Based on these findings, we conclude that, same as the diurnal variation in half-hourly PRI, the seasonal variations in daily PRI were also dominated by change in daily radiation regime. Therefore, the plant photoprotective mechanism via xanthophyll pigment interconversion might play a more important role than pigment pool size changes in determining PRI variations in mangrove ecosystems at both diurnal and seasonal scales.

Similar to the PRI-PAR correlation, PRI shows strong correlation with GPP and NEE at both diurnal (Figures 5d and 5e) and seasonal (Figures 9a and 9c) scales. This finding supports the evidence that PRI is a good indicator of photosynthetic capacity across time scales. The diurnal PRI-carbon correlation in mangrove was essentially consistent with previous studies on other vegetation types, while seasonal PRI-carbon correlations were relatively weaker (Garbulsky et al., 2011). Similar to previous studies (Zhang et al., 2017), our observations in mangrove also showed a strong link between PRI and LUE. The PRI-LUE correlation was slightly weaker (stronger) at diurnal (seasonal) scale, compared to the PRI-carbon correlation. Similar to Garbulsky et al. (2011) and S. Yang et al. (2018), there was also a PRI saturating phenomenon in our study, that is, daily PRI in mangrove tended to saturate at increasing LUE (Figure 9e) and decreasing photosynthetic capacity (Figures 9a and 9c). Further analysis reveals that the strength of the PRI-carbon and PRI-LUE correlations at diurnal scale varied with meteorological factors; that is, correlation coefficients

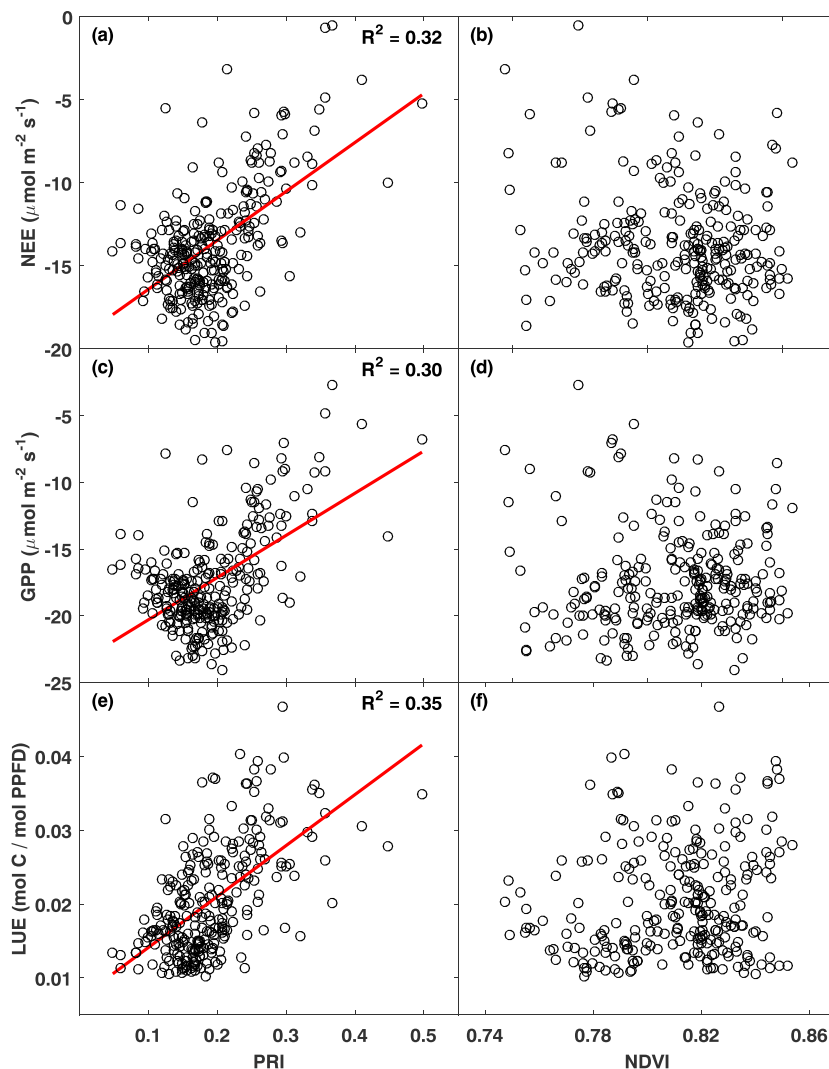


Figure 9. Scatter plots between daily spectral and carbon-related variables (a, b: net ecosystem exchange; c, d: gross primary production; and e, f: light use efficiency). (left column) Daily PRI and (right column) NDVI. NEE = net ecosystem exchange; GPP = gross primary production; LUE = light use efficiency; PRI = photochemical reflectance index; NDVI = normalized difference vegetation index.

tended to increase with under enhanced PAR, VPD, and clearness index, which is also reported by many previous studies (Magney et al., 2016; Soudani et al., 2014; Zhang et al., 2017). For example, Soudani et al. (2014) concluded that the highest PRI-LUE correlations occurred in clear or slightly cloudy conditions, showing a high sensitivity of diurnal PRI-LUE correlation to clearness index. Zhang et al. (2017) reported that the diurnal PRI-LUE correlation was sensitive to both clearness index and atmospheric water stress. The control of radiation regime and VPD (which, in fact, almost synchronously changed with radiation; Figures 4b and 4c) on diurnal PRI-LUE correlations can be explained by the fact that clear sky (high clearness index) generally had greater diurnal magnitudes of PRI, GPP, and PAR. This is also the reason why the diurnal PRI-carbon and PRI-LUE correlations were stronger in summer and spring (Table 1) when PAR, clearness index, and VPD were on average higher than other seasons (Figures 4b and 4c).

Different from physiology-related PRI, structure-related NDVI did not show any obvious correlation with photosynthetic capacity and efficiency (Figure 9), since the seasonality of NDVI was weak (0.75–0.85) in the evergreen mangrove over the study period (Figure 4a). The insensitivity of NDVI to photosynthetic parameters is consistent with the findings in previous studies on evergreen vegetation including subtropical mangrove (Nichol et al., 2006) and boreal evergreen conifers (Gamon et al., 2016). The contrasting optical

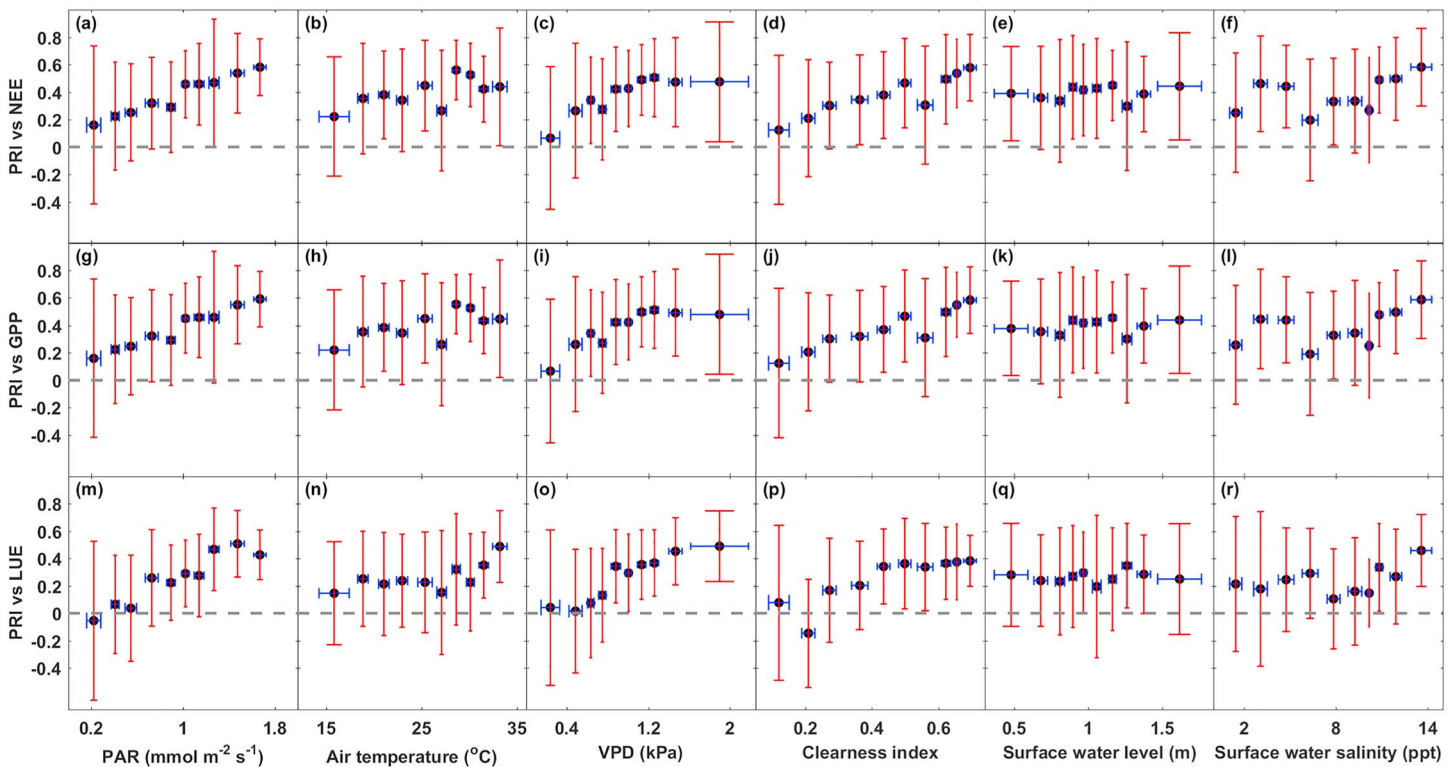


Figure 10. Influences of environmental factors on the correlations between half-hourly PRI and carbon-related variables. Pearson correlation coefficients were calculated for each single day and then grouped by environmental factors. The vertical and horizontal error bars indicate standard deviations of PRI-carbon correlations and environmental factors, respectively. (a–f) PRI versus NEE, (g–l) PRI versus GPP, and (m–r) PRI versus LUE. PRI = photochemical reflectance index; NEE = net ecosystem exchange; GPP = gross primary production; LUE = light use efficiency; PAR = photosynthetically active radiation; VPD = vapor pressure deficit.

properties reflected in PRI and NDVI support the view that evergreen vegetation with little canopy structural changes should show a weak relationship between NDVI and photosynthetic capacity but would show a strong PRI-carbon correlation (Gamon, 2015; Garbulsky et al., 2011). The contrast between relatively stable daily NDVI (Figures 4a) and strong variation in daily carbon fluxes (Figure 8b) suggests that NDVI was less useful to track mangrove photosynthetic capacity which might be mainly governed by physiological stresses rather than structural controls. Without concurrent photochemical and biochemical measurements, it is hard to reveal these physiological stresses and underlying mechanisms, but obvious correlations between PRI and photosynthetic parameters confirm that PRI can serve as a good indicator of mangrove photosynthetic capacity and efficiency.

Our data analyses of potential links between PRI and mangrove photosynthetic capacity and efficiency suffer from several uncertainties. First, although abnormal spectral signals with low illumination at dusk and dawn hours were excluded in both diurnal and seasonal analyses, we cannot rule out potential uncertainties from Sun-target-view geometry because both PRI and LUE were sensitive to radiation regime such as direct/diffuse radiation ratio and their relationship was strongly affected by canopy shading due to changing solar angle (Hall et al., 2011; Hilker et al., 2009). Future application of in situ multiangle spectral observations (Hilker et al., 2011; Zhang et al., 2017) could relieve this issue. Second, although the pigment pool size of evergreen mangrove canopy might be on average relatively stable across seasons, strong variation of daily PRI at short time scale (weeks) implies that canopy pigment contents may vary much in response to short-term environmental stresses. Concurrent measurements of PRI and relevant pigment pools are needed to confirm this deduction. Third, our analyses are only based on a 1-year period of in situ measurements which are not long enough to well characterize the high temporal variability of multiple measurements. Multiyear continuous in situ measurements are needed to better assess the ability of PRI to track mangrove photosynthetic phenology across multiple temporal scales.

5. Conclusions

Qualitative and quantitative analyses are conducted in this study to explore the potential links between PRI and mangrove photosynthetic phenology in a subtropical coastal wetland of southeastern China, based on continuous high-resolution time series measurements of spectral signals, carbon fluxes, and environmental factors. Both diurnal and seasonal variations of PRI, as well as their correlations with concurrent carbon and environmental measurements, were examined to assess the capability of PRI for tracking mangrove photosynthetic phenology. The main findings are summarized as follows. (1) Short-term PRI measurements of mangrove canopy experienced significant diurnal variation showing a U-shaped pattern with low values around noon and high values in early morning and late afternoon. (2) Long-term variation of mangrove PRI further showed strong variations during the course of a year with higher and lower values in spring and winter, respectively. (3) Diurnal and seasonal mangrove PRI variations were found significantly negatively correlated with radiation and VPD and significantly positively correlated with carbon-related parameters (GPP, NEE, and LUE). (4) The strength of mangrove PRI-carbon correlations at the diurnal scale was affected by meteorological factors with stronger correlations at enhanced radiation and VPD. (5) PRI served as a reliable indicator of mangrove carbon dynamics, including photosynthetic capacity and efficiency, while NDVI was less useful in tracking the photosynthetic phenology. (6) The radiation-induced change of pigment composition via xanthophyll photoprotective mechanism can play a more important role than the change of pigment pool size in determining mangrove PRI variations at both diurnal and seasonal scales.

To the best of our knowledge, this is the first study to explore the linkage between PRI and carbon dynamics across temporal scales in natural mangrove ecosystems using high-resolution concurrent measurements of near-surface spectral signals and EC carbon fluxes. This study demonstrated that physiology-related PRI performed better than conventional structure-related NDVI in tracking temporal dynamics of photosynthetic parameters in evergreen mangrove canopy at both diurnal and seasonal scales. Strong correlations between PRI and photosynthetic parameters ensure the potential application of PRI in characterizing mangrove carbon dynamics. Future multisite studies using more diverse spectral measurements (e.g., hyperspectral and SIF data) are needed to further assess the effectiveness of PRI as an indicator of mangrove carbon dynamics across different temporal and spatial scales.

Acknowledgments

We thank Bangqin Huang and Jianwu Tang for providing guidance on study design and thank Lingxuan Meng, Peiwen Lin, and Chenjuan Zheng for their help in the field work. We thank the Zhangjiang Estuary Mangrove National Nature Reserve for its long-term support to our ecological research program. We also thank ChinaFLUX and U.S.-China Carbon Consortium (USCCC) for helpful discussions and exchange of ideas. This study was supported by the National Natural Science Foundation of China (31600368), the Natural Science Foundation of Fujian Province, China (2017J01069), the Fundamental Research Funds for the Central Universities of China (20720180118 and 20720190104), the Key Laboratory of the Coastal and Wetland Ecosystems (WELRI201601), and the State Key Laboratory of Marine Environmental Science (MELRI1603). The data required to replicate key findings in this paper has been uploaded as supporting information.

References

- Alongi, D. M. (2009). *The energetics of mangrove forests*. Dordrecht, The Netherlands: Springer Science & Business Media.
- Alongi, D. M. (2012). Carbon sequestration in mangrove forests. *Carbon Management*, 3(3), 313–322. <https://doi.org/10.4155/cmt.12.20>
- Alongi, D. M. (2014). Carbon cycling and storage in mangrove forests. *Annual Review of Marine Science*, 6(1), 195–219. <https://doi.org/10.1146/annurev-marine-010213-135020>
- Atwood, T. B., Connolly, R. M., Almahasheer, H., Carnell, P. E., Duarte, C. M., Ewers Lewis, C. J., et al. (2017). Global patterns in mangrove soil carbon stocks and losses. *Nature Climate Change*, 7(7), 523–528. <https://doi.org/10.1038/nclimate3326>
- Baldocchi, D., Falge, E., Gu, L., Olson, R., Hollinger, D., Running, S., et al. (2001). FLUXNET: A new tool to study the temporal and spatial variability of ecosystem-scale carbon dioxide, water vapor, and energy flux densities. *Bulletin of the American Meteorological Society*, 82(11), 2415–2434. [https://doi.org/10.1175/1520-0477\(2001\)082<2415:FANTTS>2.3.CO;2](https://doi.org/10.1175/1520-0477(2001)082<2415:FANTTS>2.3.CO;2)
- Ball, M. C. (1996). *Comparative ecophysiology of mangrove forest and tropical lowland moist rainforest*, *Tropical forest plant ecophysiology*, (pp. 461–496). New York: Springer.
- Barr, J. G., Engel, V., Fuentes, J. D., Fuller, D. O., & Kwon, H. (2013). Modeling light use efficiency in a subtropical mangrove forest equipped with CO₂ eddy covariance. *Biogeosciences*, 10(3), 2145–2158. <https://doi.org/10.5194/bg-10-2145-2013>
- Barr, J. G., Engel, V., Fuentes, J. D., Zieman, J. C., O'Halloran, T. L., Smith, T. J., & Anderson, G. H. (2010). Controls on mangrove forest-atmosphere carbon dioxide exchanges in western Everglades National Park. *Journal of Geophysical Research – Biogeosciences*, 115, G02020. <https://doi.org/10.1029/2009jg001186>
- Chen, L., Wang, W., Li, Q. Q., Zhang, Y., Yang, S., Osland, M. J., et al. (2017). Mangrove species' responses to winter air temperature extremes in China. *Ecosphere*, 8(6), e01865. <https://doi.org/10.1002/ecs2.1865>
- Crass, B., Liedloff, A., Veski, P. A., Burgman, M. A., & Wintle, B. A. (2013). Hydroperiod is the main driver of the spatial pattern of dominance in mangrove communities. *Global Ecology and Biogeography*, 22(7), 806–817. <https://doi.org/10.1111/geb.12063>
- Cui, X., Liang, J., Lu, W., Chen, H., Liu, F., Lin, G., et al. (2018). Stronger ecosystem carbon sequestration potential of mangrove wetlands with respect to terrestrial forests in subtropical China. *Agricultural and Forest Meteorology*, 249, 71–80. <https://doi.org/10.1016/j.agrformet.2017.11.019>
- Demmig, B., Winter, K., Kruger, A., & Czygan, F. C. (1987). Photoinhibition and zeaxanthin formation in intact leaves: A possible role of the xanthophyll cycle in the dissipation of excess light energy. *Plant Physiology*, 84(2), 218–224. <https://doi.org/10.1104/pp.84.2.218>
- Demmig-Adams, B., Cohu, C. M., Muller, O., & Adams, W. W. (2012). Modulation of photosynthetic energy conversion efficiency in nature: From seconds to seasons. *Photosynthesis Research*, 113(1–3), 75–88. <https://doi.org/10.1007/s11120-012-9761-6>
- Filella, I., Porcar-Castell, A., Munne-Bosch, S., Bäck, J., Garbulska, M. F., & Peñuelas, J. (2009). PRI assessment of long-term changes in carotenoids/chlorophyll ratio and short-term changes in de-epoxidation state of the xanthophyll cycle. *International Journal of Remote Sensing*, 30(17), 4443–4455. <https://doi.org/10.1080/01431160802575661>

- Frankenberg, C., Fisher, J. B., Worden, J., Badgley, G., Saatchi, S. S., Lee, J. E., et al. (2011). New global observations of the terrestrial carbon cycle from GOSAT: Patterns of plant fluorescence with gross primary productivity. *Geophysical Research Letters*, *38*, L17706. <https://doi.org/10.1029/2011GL048738>
- Gamon, J. A. (2015). Reviews and syntheses: Optical sampling of the flux tower footprint. *Biogeosciences*, *12*(14), 4509–4523. <https://doi.org/10.5194/bg-12-4509-2015>
- Gamon, J. A., Huemmrich, K. F., Wong, C. Y. S., Ensminger, I., Garrity, S., Hollinger, D. Y., et al. (2016). A remotely sensed pigment index reveals photosynthetic phenology in evergreen conifers. *Proceedings of the National Academy of Sciences of the United States of America*, *113*(46), 13087–13092. <https://doi.org/10.1073/pnas.1606162113>
- Gamon, J. A., Peñuelas, J., & Field, C. B. (1992). A narrow-waveband spectral index that tracks diurnal changes in photosynthetic efficiency. *Remote Sensing of Environment*, *41*(1), 35–44. [https://doi.org/10.1016/0034-4257\(92\)90059-S](https://doi.org/10.1016/0034-4257(92)90059-S)
- Garbulsky, M. F., Peñuelas, J., Gamon, J., Inoue, Y., & Filella, I. (2011). The photochemical reflectance index (PRI) and the remote sensing of leaf, canopy and ecosystem radiation use efficiencies: A review and meta-analysis. *Remote Sensing of Environment*, *115*(2), 281–297. <https://doi.org/10.1016/j.rse.2010.08.023>
- Garbulsky, M. F., Peñuelas, J., Papale, D., Ardö, J., Goulden, M. L., Kiely, G., et al. (2010). Patterns and controls of the variability of radiation use efficiency and primary productivity across terrestrial ecosystems. *Global Ecology and Biogeography*, *19*(2), 253–267. <https://doi.org/10.1111/j.1466-8238.2009.00504.x>
- Garbulsky, M. F., Peñuelas, J., Papale, D., & Filella, I. (2008). Remote estimation of carbon dioxide uptake by a Mediterranean forest. *Global Change Biology*, *14*(12), 2860–2867. <https://doi.org/10.1111/j.1365-2486.2008.01684.x>
- Giri, C. (2016). Observation and monitoring of mangrove forests using remote sensing: Opportunities and challenges. *Remote Sensing*, *8*(9), 783. <https://doi.org/10.3390/rs8090783>
- Gitelson, A. A., & Gamon, J. A. (2015). The need for a common basis for defining light-use efficiency: Implications for productivity estimation. *Remote Sensing of Environment*, *156*, 196–201. <https://doi.org/10.1016/j.rse.2014.09.017>
- Hall, F. G., Hilker, T., & Coops, N. C. (2011). PHOTOSYNSTAT, photosynthesis from space: Theoretical foundations of a satellite concept and validation from tower and spaceborne data. *Remote Sensing of Environment*, *115*(8), 1918–1925. <https://doi.org/10.1016/j.rse.2011.03.014>
- Hartel, H., Lokstein, H., Grimm, B., & Rank, B. (1996). Kinetic studies on the xanthophyll cycle in barley leaves (influence of antenna size and relations to nonphotochemical chlorophyll fluorescence quenching). *Plant Physiology*, *110*(2), 471–482. <https://doi.org/10.1104/pp.110.2.471>
- Hilker, T., Coops, N. C., Coggins, S. B., Wulder, M. A., Brown, M., Black, T. A., et al. (2009). Detection of foliage conditions and disturbance from multi-angular high spectral resolution remote sensing. *Remote Sensing of Environment*, *113*(2), 421–434. <https://doi.org/10.1016/j.rse.2008.10.003>
- Hilker, T., Gitelson, A., Coops, N. C., Hall, F. G., & Black, T. A. (2011). Tracking plant physiological properties from multi-angular tower-based remote sensing. *Oecologia*, *165*(4), 865–876. <https://doi.org/10.1007/s00442-010-1901-0>
- Howard, J., Sutton-Grier, A., Herr, D., Kleypas, J., Landis, E., Mcleod, E., et al. (2017). Clarifying the role of coastal and marine systems in climate mitigation. *Frontiers in Ecology and the Environment*, *15*(1), 42–50. <https://doi.org/10.1002/fee.1451>
- Huete, A., Didan, K., Miura, T., Rodriguez, E. P., Gao, X., & Ferreira, L. G. (2002). Overview of the radiometric and biophysical performance of the MODIS vegetation indices. *Remote Sensing of Environment*, *83*(1-2), 195–213. [https://doi.org/10.1016/S0034-4257\(02\)00096-2](https://doi.org/10.1016/S0034-4257(02)00096-2)
- Jiang, S., Lu, H., Liu, J., Lin, Y., Dai, M., & Yan, C. (2018). Influence of seasonal variation and anthropogenic activity on phosphorus cycling and retention in mangrove sediments: A case study in China. *Estuarine, Coastal and Shelf Science*, *202*, 134–144. <https://doi.org/10.1016/j.ecss.2017.12.011>
- Joiner, J., Yoshida, Y., Vasilkov, A. P., Schaefer, K., Jung, M., Guanter, L., et al. (2014). The seasonal cycle of satellite chlorophyll fluorescence observations and its relationship to vegetation phenology and ecosystem atmosphere carbon exchange. *Remote Sensing of Environment*, *152*, 375–391. <https://doi.org/10.1016/j.rse.2014.06.022>
- Le Quéré, C., Raupach, M. R., Canadell, J. G., Marland, G., Bopp, L., Ciais, P., et al. (2009). Trends in the sources and sinks of carbon dioxide. *Nature Geoscience*, *2*(12), 831. <https://doi.org/10.1038/ngeo689>
- Li, Q., Lu, W., Chen, H., Luo, Y., & Lin, G. (2014). Differential responses of net ecosystem exchange of carbon dioxide to light and temperature between spring and neap tides in subtropical mangrove forests. *The Scientific World Journal*, *2014*, 943697. <https://doi.org/10.1155/2014/943697>
- Lin, P. (2001). *The comprehensive report of science investigation on the natural reserve of mangrove wetland of Zhangjiang Estuary in Fujian*. Xiamen, China: Xiamen University Press.
- Lloyd, J., & Taylor, J. A. (1994). On the temperature dependence of soil respiration. *Functional Ecology*, *8*(3), 315–323. <https://doi.org/10.2307/2389824>
- Magney, T. S., Vierling, L. A., Eitel, J. U. H., Huggins, D. R., & Garrity, S. R. (2016). Response of high frequency photochemical reflectance index (PRI) measurements to environmental conditions in wheat. *Remote Sensing of Environment*, *173*, 84–97. <https://doi.org/10.1016/j.rse.2015.11.013>
- Monteith, J. L., & Moss, C. J. (1977). Climate and the efficiency of crop production in Britain [and discussion]. *Philosophical Transactions of the Royal Society of London. Series B, Biological Sciences*, *281*(980), 277–294. <https://doi.org/10.1098/rstb.1977.0140>
- Murray, F. W. (1966). On the computation of saturation vapor pressure, RAND CORP SANTA MONICA CALIF.
- Myneni, R. B., & Williams, D. L. (1994). On the relationship between FAPAR and NDVI. *Remote Sensing of Environment*, *49*(3), 200–211. [https://doi.org/10.1016/0034-4257\(94\)90016-7](https://doi.org/10.1016/0034-4257(94)90016-7)
- Nellemann, C., & Corcoran, E. (2009). Blue carbon: The role of healthy oceans in binding carbon: A rapid response assessment. UNEP/Earthprint.
- Nichol, C. J., Drolet, G., Porcar-Castell, A., Wade, T., Sabater, N., Middleton, E. M., et al. (2019). Diurnal and seasonal solar induced chlorophyll fluorescence and photosynthesis in a boreal Scots pine canopy. *Remote Sensing*, *11*(3), 273. <https://doi.org/10.3390/rs11030273>
- Nichol, C. J., Rascher, U., Matsubara, S., & Osmond, B. (2006). Assessing photosynthetic efficiency in an experimental mangrove canopy using remote sensing and chlorophyll fluorescence. *Trees*, *20*(1), 9–15. <https://doi.org/10.1007/s00468-005-0005-7>
- Peguero-Pina, J. J., Gil-Pelegrín, E., & Morales, F. (2013). Three pools of zeaxanthin in *Quercus coccifera* leaves during light transitions with different roles in rapidly reversible photoprotective energy dissipation and photoprotection. *Journal of Experimental Botany*, *64*(6), 1649–1661. <https://doi.org/10.1093/jxb/ert024>

- Porcar-Castell, A., Tyystjärvi, E., Atherton, J., van der Tol, C., Flexas, J., Pfündel, E. E., et al. (2014). Linking chlorophyll a fluorescence to photosynthesis for remote sensing applications: Mechanisms and challenges. *Journal of Experimental Botany*, *65*(15), 4065–4095. <https://doi.org/10.1093/jxb/eru191>
- Reichstein, M., Falge, E., Baldocchi, D., Papale, D., Aubinet, M., Berbigier, P., et al. (2005). On the separation of net ecosystem exchange into assimilation and ecosystem respiration: Review and improved algorithm. *Global Change Biology*, *11*(9), 1424–1439. <https://doi.org/10.1111/j.1365-2486.2005.001002.x>
- Ruimy, A., Saugier, B., & Dedieu, G. (1994). Methodology for the estimation of terrestrial net primary production from remotely sensed data. *Journal of Geophysical Research*, *99*(D3), 5263–5283. <https://doi.org/10.1029/93JD03221>
- Running, S. W., Nemani, R. R., Heinsch, F. A., Zhao, M., Reeves, M., & Hashimoto, H. (2004). A continuous satellite-derived measure of global terrestrial primary production. *BioScience*, *54*(6), 547–560. [https://doi.org/10.1641/0006-3568\(2004\)054\[0547:ACSMOG\]2.0.CO;2](https://doi.org/10.1641/0006-3568(2004)054[0547:ACSMOG]2.0.CO;2)
- Shrestha, S., Brueck, H., & Asch, F. (2012). Chlorophyll index, photochemical reflectance index and chlorophyll fluorescence measurements of rice leaves supplied with different N levels. *Journal of Photochemistry and Photobiology B: Biology*, *113*, 7–13. <https://doi.org/10.1016/j.jphotobiol.2012.04.008>
- Simard, M., Fatoyinbo, L., Smetanka, C., Rivera-Monroy, V. H., Castañeda-Moya, E., Thomas, N., & van der Stocken, T. (2019). Mangrove canopy height globally related to precipitation, temperature and cyclone frequency. *Nature Geoscience*, *12*(1), 40–45. <https://doi.org/10.1038/s41561-018-0279-1>
- Song, C., White, B. L., & Heumann, B. W. (2011). Hyperspectral remote sensing of salinity stress on red (*Rhizophora mangle*) and white (*Laguncularia racemosa*) mangroves on Galapagos Islands. *Remote Sensing Letters*, *2*(3), 221–230. <https://doi.org/10.1080/01431161.2010.514305>
- Soudani, K., Hmimina, G., Dufrene, E., Berveiller, D., Delpierre, N., Ourcival, J. M., et al. (2014). Relationships between photochemical reflectance index and light-use efficiency in deciduous and evergreen broadleaf forests. *Remote Sensing of Environment*, *144*, 73–84. <https://doi.org/10.1016/j.rse.2014.01.017>
- Tian, Y., Woodcock, C. E., Wang, Y., Privette, J. L., Shabanov, N. V., Zhou, L., et al. (2002). Multiscale analysis and validation of the MODIS LAI product: I. Uncertainty assessment. *Remote Sensing of Environment*, *83*(3), 414–430. [https://doi.org/10.1016/S0034-4257\(02\)00047-0](https://doi.org/10.1016/S0034-4257(02)00047-0)
- Tucker, C. J., Townshend, J. R., & Goff, T. E. (1985). African land-cover classification using satellite data. *Science*, *227*(4685), 369–375. <https://doi.org/10.1126/science.227.4685.369>
- Verhoeven, A. (2014). Sustained energy dissipation in winter evergreens. *New Phytologist*, *201*(1), 57–65. <https://doi.org/10.1111/nph.12466>
- Wagle, P., Gowda, P. H., Xiao, X., & Anup, K. C. (2016). Parameterizing ecosystem light use efficiency and water use efficiency to estimate maize gross primary production and evapotranspiration using MODIS EVI. *Agricultural and Forest Meteorology*, *222*, 87–97. <https://doi.org/10.1016/j.agrformet.2016.03.009>
- Walther, S., Voigt, M., Thum, T., Gonsamo, A., Zhang, Y., Köhler, P., et al. (2016). Satellite chlorophyll fluorescence measurements reveal large-scale decoupling of photosynthesis and greenness dynamics in boreal evergreen forests. *Global Change Biology*, *22*(9), 2979–2996. <https://doi.org/10.1111/gcb.13200>
- Wong, C. Y. S., & Gamon, J. A. (2015). The photochemical reflectance index provides an optical indicator of spring photosynthetic activation in evergreen conifers. *New Phytologist*, *206*(1), 196–208. <https://doi.org/10.1111/nph.13251>
- Xiao, X. M., Hollinger, D., Aber, J., Goltz, M., Davidson, E. A., Zhang, Q., & Moore, B. III (2004). Satellite-based modeling of gross primary production in an evergreen needleleaf forest. *Remote Sensing of Environment*, *89*(4), 519–534. <https://doi.org/10.1016/j.rse.2003.11.008>
- Yang, K., Ryu, Y., Dechant, B., Berry, J. A., Hwang, Y., Jiang, C., et al. (2018). Sun-induced chlorophyll fluorescence is more strongly related to absorbed light than to photosynthesis at half-hourly resolution in a rice paddy. *Remote Sensing of Environment*, *216*, 658–673. <https://doi.org/10.1016/j.rse.2018.07.008>
- Yang, S., Wang, L., Shi, C., & Lu, Y. (2018). Evaluating the relationship between the photochemical reflectance index and light use efficiency in a mangrove forest with *Spartina alterniflora* invasion. *International Journal of Applied Earth Observation and Geoinformation*, *73*, 778–785. <https://doi.org/10.1016/j.jag.2018.08.014>
- Yuan, W. P., Liu, S., Zhou, G., Zhou, G., Tieszen, L. L., Baldocchi, D., et al. (2007). Deriving a light use efficiency model from eddy covariance flux data for predicting daily gross primary production across biomes. *Agricultural and Forest Meteorology*, *143*(3-4), 189–207. <https://doi.org/10.1016/j.agrformet.2006.12.001>
- Zhang, C., Kovacs, J., Wachowiak, M., & Flores-Verdugo, F. (2013). Relationship between hyperspectral measurements and mangrove leaf nitrogen concentrations. *Remote Sensing*, *5*(2), 891–908. <https://doi.org/10.3390/rs5020891>
- Zhang, Q., Ju, W., Chen, J., Wang, H., Yang, F., Fan, W., et al. (2015). Ability of the photochemical reflectance index to track light use efficiency for a sub-tropical planted coniferous forest. *Remote Sensing*, *7*(12), 16938–16962. <https://doi.org/10.3390/rs71215860>
- Zhang, Q., M. Chen, J., Ju, W., Wang, H., Qiu, F., Yang, F., et al. (2017). Improving the ability of the photochemical reflectance index to track canopy light use efficiency through differentiating sunlit and shaded leaves. *Remote Sensing of Environment*, *194*, 1–15. <https://doi.org/10.1016/j.rse.2017.03.012>
- Zhu, X., He, H., Liu, M., Yu, G., Sun, X., & Gao, Y. (2010). Spatio-temporal variation of photosynthetically active radiation in China in recent 50 years. *Journal of Geographical Sciences*, *20*(6), 803–817. <https://doi.org/10.1007/s11442-010-0812-7>
- Zhu, X., Hou, Y., Weng, Q., & Chen, L. (2019). Integrating UAV optical imagery and LiDAR data for assessing the spatial relationship between mangrove and inundation across a subtropical estuarine wetland. *ISPRS Journal of Photogrammetry and Remote Sensing*, *149*, 146–156. <https://doi.org/10.1016/j.isprsjsprs.2019.01.021>